JACS
JOURNAL OF THE AMERICAN CHEMICAL SOCIETY
Article
pubs.acs.org/JACS

Spectroscopic and Redox Studies of Valence-Delocalized $[Fe_2S_2]^+$ Centers in Thioredoxin-like Ferredoxins

Sowmya Subramanian,[†,∥] Evert C. Duin,[†,⊥] Sarah E. J. Fawcett,[‡] Fraser A. Armstrong,[‡] Jacques Meyer,[§] and Michael K. Johnson*[,†]

[†]Department of Chemistry and Center for Metalloenzyme Studies, University of Georgia, Athens, Georgia 30602, United States
[‡]Department of Chemistry, University of Oxford, South Parks Road, Oxford, OX1 3QR, United Kingdom
[§]1, Allée Docteur Calmette, 38130 Échirolles, France

Supporting Information

ABSTRACT: Reduced forms of the C56S and C60S variants of the thioredoxin-like *Clostridium pasteurianum* $[Fe_2S_2]$ ferredoxin (*Cp*Fd) provide the only known examples of valence-delocalized $[Fe_2S_2]^+$ clusters, which constitute a fundamental building block of all higher nuclearity Fe−S clusters. In this work, we have revisited earlier work on the *Cp*Fd variants and carried out redox and spectroscopic studies on the $[Fe_2S_2]^{2+,+}$ centers in wild-type and equivalent variants of the highly homologous and structurally characterized *Aquifex aeolicus* ferredoxin 4 (*Aae*Fd4) using EPR, UV−visible−NIR absorption, CD and variable-temperature MCD, and protein−film electrochemistry. The results indicate that the $[Fe_2S_2]^+$ centers in the equivalent *Aae*Fd4 and *Cp*Fd variants reversibly interconvert between similar valence-localized S = 1/2 and valence-delocalized S = 9/2 forms as a function of pH, with pK_a values in the range 8.3−9.0, because of protonation of the coordinated serinate residue. However, freezing high-pH samples results in partial or full conversion from valence-delocalized S = 9/2 to valence-localized S = 1/2 $[Fe_2S_2]^+$ clusters. MCD saturation magnetization data for valence-delocalized S = 9/2 $[Fe_2S_2]^+$ centers facilitated determination of transition polarizations and thereby assignments of low-energy MCD bands associated with the Fe−Fe interaction. The assignments provide experimental assessment of the double exchange parameter, B, for valence-delocalized $[Fe_2S_2]^+$ centers and demonstrate that variable-temperature MCD spectroscopy provides a means of detecting and investigating the properties of valence-delocalized S = 9/2 $[Fe_2S_2]^+$ fragments in higher nuclearity Fe−S clusters. The origin of valence delocalization in thioredoxin-like ferredoxin Cys-to-Ser variants and Fe−S clusters in general is discussed in light of these results.

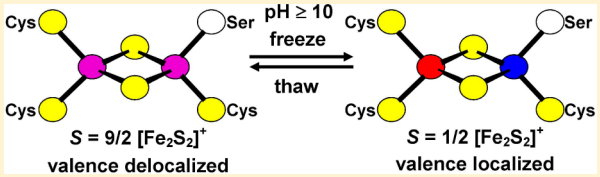

INTRODUCTION

Valence delocalization is an intrinsic property of numerous high-nuclearity biological Fe−S clusters, e.g., $[Fe_3S_4]^0$, $[Fe_4S_4]^{3+,2+,+}$, $[Fe_8S_7]^{4+,3+}$ clusters, and is important for understanding ground and excited state electronic properties and facilitating rapid electron transport by minimizing reorganization energy associated with oxidation/reduction.[1,2] It is therefore important to understand the origins of valence delocalization in order to interpret the electronic properties of Fe−S clusters and to rationalize the thermodynamics and kinetics of intercluster electron transfer. On the basis of Fe−S cluster biogenesis studies, $Fe_2(\mu_2\text{-}S)_2$ units ($[Fe_2S_2]$) constitute the basic building blocks of all Fe−S clusters,[3] and spectroscopic studies have demonstrated that valence-delocalized $[Fe_2S_2]^+$ fragments with ferromagnetically coupled S = 9/2 ground states are intrinsic components of all homometallic and heterometallic high nuclearity Fe−S clusters in at least one oxidation state.[4,5] However, understanding the origin and properties of valence-delocalized $[Fe_2S_2]^+$ units has been impeded by the fact that all known synthetic and naturally occurring biological $[Fe_2S_2]^+$ centers are valence localized and exhibit S = 1/2 ground states as a result of antiferromagnetic coupling.[6]

Valence localization in the reduced cluster is promoted by large localization energy (ΔE), which includes contributions from vibronic coupling and the magnitude of the difference in site redox potentials, and is manifest by strong antiferromagnetic exchange interaction, which restricts delocalization of the extra electron by requiring a spin flip to visit both Fe sites. In contrast, valence delocalization is expected to require a significant Fe−Fe interaction, such that the resonance delocalization energy overwhelms the localization energy, and results in the switch to ferromagnetic exchange interaction and a S = 9/2 ground state so that the extra electron can visit both Fe sites without undergoing a spin flip. Hence, valence delocalization in $[Fe_2S_2]^+$ clusters requires spin-dependent resonance delocalization and is parametrized by the double exchange parameter, B, where $10B = 2\beta$, and β is the classical resonance energy that is more familiar to chemists. The ground state properties of a $[Fe_2S_2]^+$ cluster fragment depend on the

Received: February 19, 2015
Published: March 19, 2015

ACS Publications © 2015 American Chemical Society

DOI: 10.1021/jacs.5b01869
J. Am. Chem. Soc. 2015, 137, 4567−4580

relative magnitudes of Heisenberg–Dirac–vanVleck (J) exchange and double exchange (B) terms and result in energies $E = -JS(S + 1) \pm B(S + {}^{1}/_{2})$.[7] This simple model neglects vibronic interactions and assumes that the valence-localized species with the extra electron on the two iron sites, Fe_A and Fe_B, are isoenergetic. As the extent of resonance delocalization (B/J) increases, the ground state changes from $S = 1/2$ to 9/2 in integer steps, becoming $S = 9/2$ for $|B/J| > 9$. Inclusion of the factors responsible for valence localization, i.e., vibronic coupling and inequivalence in the energies of the valence trapped species, decreases the B/J range in which the ground state has $S = \pm 3/2$ or $\pm 7/2$. This diminishes the likelihood of observing these intermediate-spin ground states and leads toward a situation in which the ground state changes directly from valence-localized $S = 1/2$ to valence-delocalized $S = 9/2$ with increasing B/J. Hence the absolute value of B/J and the energetic factors responsible for valence localization determine both the ground state spin and the extent of valence delocalization.

The lack of examples of magnetically isolated, valence-delocalized $[Fe_2S_2]^+$ clusters has impeded understanding of the structural and electronic determinants of valence delocalization. Hence, the observation of $S = 9/2$ valence-delocalized $[Fe_2S_2]^+$ clusters in variants of *Clostridium pasteurianum* $[Fe_2S_2]$ ferredoxin (*Cp*Fd) in which either of the cysteines coordinating the reducible Fe site were substituted with serine (C56S and C60S) provided the opportunity to characterize the properties of a valence-delocalized $[Fe_2S_2]^+$ cluster and assess the determinants of valence delocalization in these variants. The initial discovery of $S = 9/2$ $[Fe_2S_2]^+$ clusters in these variants came from EPR and variable-temperature magnetic circular dichroism (VTMCD) studies of dithionite-reduced samples at alkaline pH which revealed a mixture of $S = 1/2$ and 9/2 $[Fe_2S_2]^+$ clusters.[5,8] Moreover, the similarity in the NIR electronic transitions of the $S = 9/2$ component with those of clusters known to contain valence-delocalized $[Fe_2S_2]^+$ fragments as revealed by VTMCD suggested valence-delocalized $[Fe_2S_2]^+$ clusters.[5,8] Definitive evidence for complete valence delocalization (Robin–Day class 3) for the $S = 9/2$ $[Fe_2S_2]^+$ clusters was subsequently provided by Mössbauer spectroscopy.[9] In addition, Mössbauer and saturation magnetization studies indicated that the ratio of $S = 9/2$ and 1/2 $[Fe_2S_2]^+$ clusters was maximally 1:1 even at pH 11 and interestingly indicated that the $S = 1/2$ component at alkaline pH is valence localized at low temperatures but becomes valence delocalized without a spin-state change at high temperatures (transition temperature of ~100 K).[10]

Structural data are not available for *Clostridium pasteurianum* $[Fe_2S_2]$ ferredoxin, which is a member of the thioredoxin-like class of ferredoxins.[11] However, high resolution crystal structures are available for the oxidized form of a close homolog of the *Cp*Fd, the wild-type (WT) $[Fe_2S_2]$ ferredoxin-4 from the hyperthermophilic bacterium *Aquifex aeolicus* (*Aae*Fd4) (solved at 1.5 Å resolution), and the corresponding oxidized Cys-to-Ser variants, C55S and C59S (solved at 1.25 Å and 1.05 Å resolution, respectively).[12,13] The crystallographic data indicated a thioredoxin-like fold and confirmed serinate ligation to the oxidized $[Fe_2S_2]^{2+}$ cluster in both variants. Moreover, serinate ligation was accompanied by a significant distortion in the $[Fe_2S_2]$ core and shortening of the Fe–Fe distance by 0.04 Å which was proposed to be an important determinant for valence delocalization in the reduced samples. However, there is currently no evidence in support of a valence-delocalized $[Fe_2S_2]^+$ cluster in reduced samples of the C55S and C59S variants of *Aae*Fd4. To remedy this situation, we report here a detailed comparison of the spectroscopic and redox properties of WT and the corresponding Cys-to-Ser variants of *Cp*Fd and *Aae*Fd4 using protein film electrochemistry and the combination of EPR and UV–visible absorption, CD, and VTMCD spectroscopies. The implications of the results for the properties and origin of valence-delocalized $S = 9/2$ $[Fe_2S_2]^+$ clusters in the reduced Cys-to-Ser variants of these ferredoxins are discussed.

MATERIALS AND METHODS

Sample Preparation and Redox Measurements. WT and variant forms of *Cp*Fd and *Aae*Fd4 were prepared as previously described.[14,15] Sample preparation and handling were carried out under anaerobic conditions in a Vacuum Atmospheres glovebox under an argon atmosphere (<5 ppm O_2). Samples of as-prepared and dithionite-reduced WT and variant forms of *Aae*Fd4 variants were prepared at pH 7.0–8.0 and at pH 11.0–12.0, and 50% (v/v) ethylene glycol was used as the glassing agent for VTMCD studies. Low pH samples were prepared in 200 mM Tris-HCl buffer with 0.1 M NaCl, and high pH samples were prepared in 200 mM CAPS buffer with 0.1 M NaCl. Samples of as-prepared and dithionite-reduced WT and variant forms of *Cp*Fd were prepared in 200 mM MES buffer with 0.2 M NaCl at pH 6.0, 200 mM Tris-HCl buffer with 0.1 M NaCl at pH 7.0, or 200 mM CAPS buffer with 0.1 M NaCl at pH 11.0. Samples used for VTMCD spectroscopy contained 50% (v/v) ethylene glycol or glycerol as the glassing agent. Samples of the *Aae*Fd4 and *Cp*Fd variants for RTMCD (room-temperature magnetic circular dichroism) studies were prepared in a mixed buffer system (50 mM Tris, 50 mM CHES, 50 mM CAPS, and 50 mM phosphate) with 0.1 M NaCl and were adjusted to pH 7 or 12. Reduction potentials were determined by direct cyclic voltammetry of protein samples adsorbed on modified graphite electrodes under anaerobic conditions (<1.5 ppm of O_2). An all-glass three-electrode cell was used for all measurements, and voltammograms were recorded with an Autolab electrochemical analyzer (Eco-Chemie). Specifically, reduction potentials and their pH dependence were determined by applying 100 μM solution of the protein as a film on the electrode with 200 μg mL^{-1} of polymyxin as coadsorbate, then using the protein-modified electrode to record voltammograms in solutions of varying pH based on 10 mM mixed buffer and 0.1 M NaCl. Voltammograms were recorded at 0 °C with scan rates below 20 mV s^{-1}.

Spectroscopic Methods. UV–visible absorption and CD spectra were recorded in anaerobic 1 mm cuvettes using a Shimadzu 3101 PC spectrophotometer and a Jasco J-715 spectropolarimeter, respectively. UV–visible–NIR VTMCD spectra were recorded on samples containing 50% (v/v) ethylene glycol or glycerol using Jasco J-715 and J-730 spectropolarimeters interfaced to an Oxford Instruments Spectromag 4000 (0–7 T) split coil superconducting magnet (sample temperatures of 1.5–300 K) using the published protocols.[16,17] Variable-field and variable-temperature (VHVT) MCD saturation magnetization data were collected at sweep rates of 0.78 T/min from 0 to 6 T at fixed temperatures and analyzed according to the published procedures,[18] using software supplied by Prof. Edward I. Solomon (Stanford University). RTMCD spectra in the UV–visible–NIR region were recorded using a Jasco J-730 spectropolarimeter interfaced to a Jasco MCD-1B electromagnet (0–1.5 T). X-band EPR spectra were recorded on a Bruker Instruments ESP 300E spectrometer equipped with an ER-4116 dual mode cavity and an Oxford Instruments ESR 900 flow cryostat (4.2–300 K). $S = 1/2$ resonances were quantified under nonsaturating conditions by double integration against a 1 mM Cu–EDTA standard. Spin Hamiltonian parameters for $S = 9/2$ resonances were determined using the Rhombo program provided by Dr. Wilfred Hagen, Delft University, The Netherlands.

DOI: 10.1021/jacs.5b01869
J. Am. Chem. Soc. 2015, 137, 4567–4580

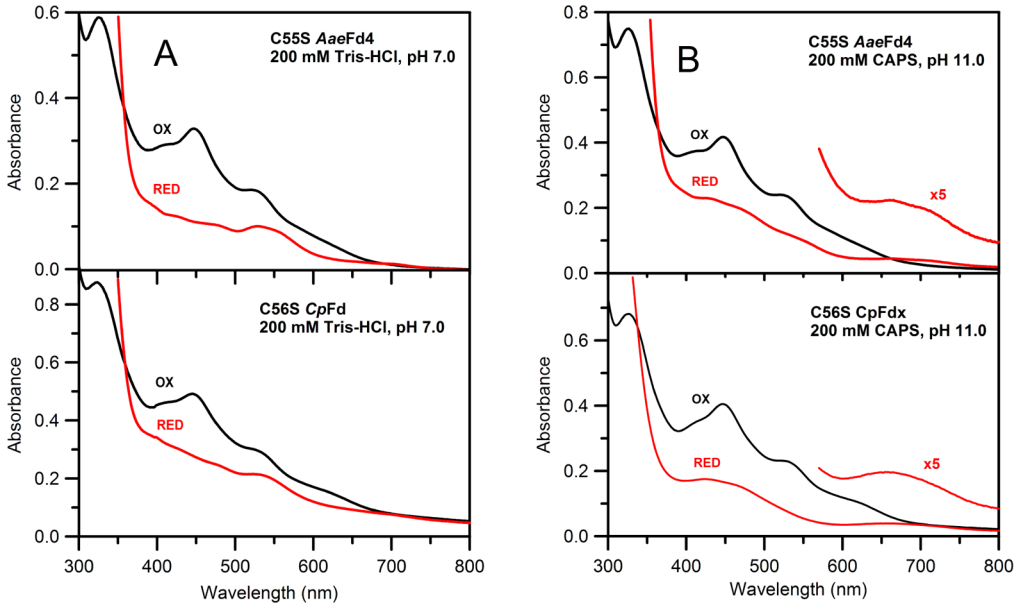

Figure 1. (A) UV−visible absorption spectra of oxidized and dithionite-reduced C55S *Aae*Fd4 (0.34 mM) and C56S *Cp*Fd (0.46 mM) in 200 mM Tris-HCl buffer with 0.1 M NaCl at pH 7.0. (B) UV−visible absorption spectra of oxidized and dithionite-reduced C55S *Aae*Fd4 (0.43 mM) and C56S *Cp*Fd (0.42 mM) in 200 mM CAPS buffer with 0.1 M NaCl at pH 11.0. All spectra are recorded in 0.1 cm cuvettes.

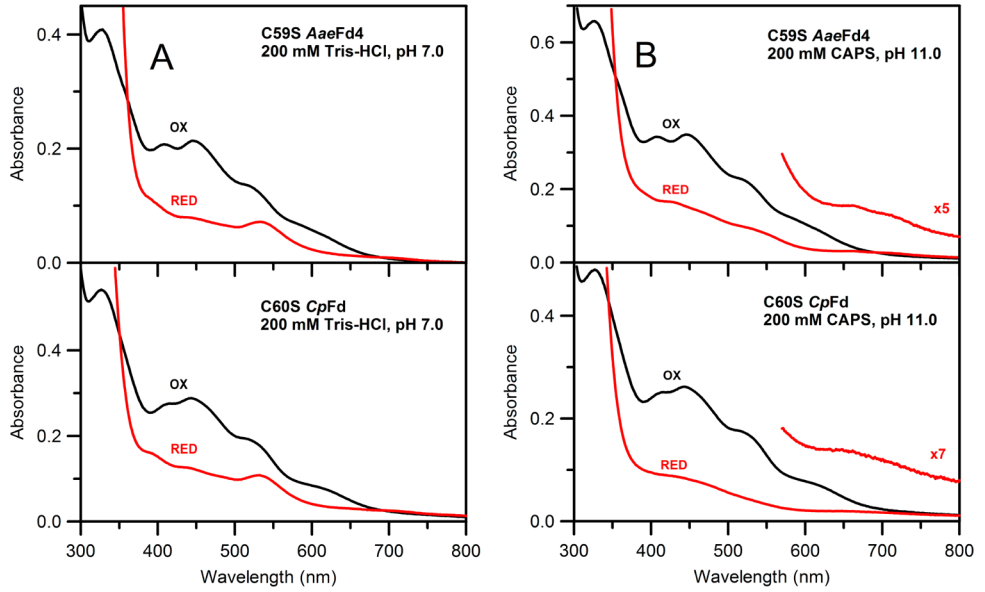

Figure 2. (A) UV−visible absorption spectra of oxidized and dithionite-reduced C59S *Aae*Fd4 (0.22 mM) and C60S *Cp*Fd (0.33 mM) in 200 mM Tris-HCl buffer with 0.1 M NaCl at pH 7.0. (B) UV−visible absorption spectra of oxidized and dithionite-reduced C59S *Aae*Fd4 (0.36 mM) and C60S *Cp*Fd (0.27 mM) in 200 mM CAPS buffer with 0.1 M NaCl at pH 11.0. All spectra are recorded in 0.1 cm cuvettes.

RESULTS

UV−Visible Absorption. The UV−visible absorption spectra of the oxidized and dithionite-reduced WT *Aae*Fd4 at pH 7.0 (Figure S1) are identical to those reported previously for WT *Cp*Fd, with prominent bands at 335, 425, 464, and 545 nm for the oxidized $[Fe_2S_2]^{2+}$ center and a band around 550 nm characteristic of a valence-localized, dithionite-reduced $[Fe_2S_2]^{+}$ center.[14,19] Neither oxidized nor dithionite-reduced WT *Aae*Fd4 and *Cp*Fd exhibited any change in absorption properties as a function of pH in the range pH 6−11 (Figure S1). The electronic spectra of the oxidized Cys-to-Ser variants, C55S and C59S *Aae*Fd4, were also very similar to the analogous C56S and C60S *Cp*Fd variants, with prominent bands around 320, 415, 440, and 530 nm, and were independent of pH over the range pH 6−11 (Figures 1 and 2). The observed spectra are characteristic of a $[Fe_2S_2]^{2+}$ ferredoxin, and the blue shifts in the absorption spectra of the variants compared to WT are consistent with serinate ligation of the oxidized $[Fe_2S_2]^{2+}$ cluster.[19] In contrast, the absorption spectra of the dithionite-reduced variants at high pH (11−12) are quite different from those observed at neutral pH. The band at 550 nm that is characteristic of $S = 1/2$ $[Fe_2S_2]^{+}$ valence-localized centers in the dithionite-reduced variants at neutral pH is replaced by broad absorption bands in 400−500 and 600−750 nm regions at high pH (Figures 1 and 2). The drastic change in the absorption properties of the reduced

DOI: 10.1021/jacs.5b01869
J. Am. Chem. Soc. 2015, 137, 4567−4580

*Aae*Fd4 variants as a function of pH is similar to that observed for the equivalent *Cp*Fd variants and suggests the presence of different $[Fe_2S_2]^+$ centers with distinct excited state electronic properties at low and high pH in both sets of ferredoxin Cys-to-Ser variants.

Redox Properties and CD Spectra. The redox properties of protein-bound $[Fe_2S_2]$ clusters depend on a number of factors such as the nature of the ligating residues, extent of solvent exposure at the reducible iron site, and asymmetry in hydrogen bonding interactions and the overall cluster environment.[6] A Cys-to-Ser mutation at the reducible iron site, while other factors remain the same, is expected to cause a negative shift in midpoint potential (ΔE_m) as a consequence of the more electronegative serinate stabilizing the Fe(III) oxidation state. For example, in *E. coli* fumarate reductase, the midpoint potentials of the $[Fe_2S_2]^{2+,+}$ centers in the C57S and C62S variants are shifted to −103 and −243 mV, respectively, versus NHE at pH 7.0, compared to a midpoint potential of −79 mV for WT.[20] The results of extensive crystallographic, site-directed mutagenesis and spectroscopic studies of the $[Fe_2S_2]$ center in *Cp*Fd and *Aae*Fd4 have definitively established that the Cys56/Cys60 and Cys55/Cys59 equivalent pairs of cysteines serve as ligands to the reducible iron.[12,13,19,21] Hence the reduction potentials of WT, C56S and C60S *Cp*Fd and WT, C55S and C59S *Aae*Fd4 were determined at pH 7.0. As expected, the mutations resulted in a 100−102 mV decrease in midpoint potential for the *Cp*Fd variants compared to the WT (E_m = −280 mV versus NHE at pH 7.0) and a 100−140 mV decrease in midpoint potential for the *Aae*Fd4 variants compared to the WT (E_m = −262 mV versus NHE at pH 7.0); see Table 1. The

Table 1. Redox Potentials[a] and pK_a Values[b] for WT and Variant Forms of *Aae*Fd4 and *Cp*Fd.

	redox potential (mV)	pK_a
*Aae*Fd4	−280 ± 10	
*Aae*Fd4 C55S variant	−380 ± 10	9.0
*Aae*Fd4 C59S variant	−420 ± 10	8.3
*Cp*Fd	−262 ± 10	
*Cp*Fd C56S variant	−364 ± 10	8.7
*Cp*Fd C60S variant	−362 ± 10	8.9

[a]The redox potentials of the *Aae*Fd4 and *Cp*Fd WT and variant forms were determined by film voltammetry at pH 7.0 versus SHE at 0 °C. [b]pK_a values for reduced *Aae*Fd4 variants were determined by monitoring the pH dependence via CD spectrophotometric titrations (Figure 4). pK_a values for reduced *Cp*Fd variants were determined by monitoring the pH dependence via film voltammetry (Figure 3).

reduction potentials of WT and the Cys-to-Ser variants of *Cp*Fd were monitored as a function of pH by film voltammetry at 0 °C. While the WT protein showed no significant change in reduction potential (average of peak positions for scans in each direction) in the pH range 5−10, the C56S and the C60S variants showed a steady decrease with increasing pH, reaching a constant value of approximately −460 mV at pH > 10 (Figure 3). A nonlinear regression fit of the data in Figure 3 was performed using eq 1, where $E^{0\prime}$ is the reduction potential measured as a function of pH, $E^{0\prime}_{alk}$ is the reduction potential in the limit of high pH, n is the number of electrons transferred, and y is the number of protons transferred with a dissociation constant, K_a.

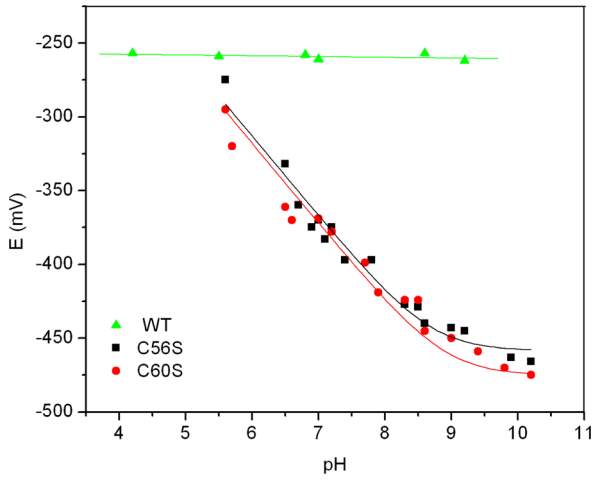

Figure 3. Dependence of the midpoint potential (mV vs NHE) of the WT (green ▲) and the C56S (■) and C60S (red ●) variants of *Cp*Fd on pH, as determined by protein film voltammetry. The solid lines show nonlinear regression fits to eq 1 for a single protonation event that occurs with a pK_a of 8.7 and 8.9 for the C56S and C60S variants, respectively.

$$E^{0\prime} = E^{0\prime}_{alk} + \frac{RT}{nF}\ln\left[1 + \frac{([H]^+)^y}{K_a}\right] \quad (1)$$

Results of the fits show that the reduction potentials of C56S and C60S variants show a strong pH dependence with a drop of about −50 mV/pH unit in the pH range 6−8, close to the theoretical value of −54 mV for a one proton/one electron reaction. Hence the reduced clusters are associated with a single protonation event that occurs with a pK_a of 8.7 and 8.9 for the C56S and C60S variants, respectively. Since serinate is a good candidate for protonation with pK_a ≈ 9.0 and serinate is known to ligate the reducible Fe site of the $[Fe_2S_2]^{2+}$ center based on crystallographic data for the equivalent mutants in *Aae*Fd4,[21] the dramatic pH-induced changes in the excited state electronic properties of the reduced cluster are interpreted in terms of protonation of the serinate ligand.

CD spectroscopy rather than film voltammetry was used to determine the pK_a of the reduced clusters in the C55S and C59S variants of *Aae*Fd4. The CD spectra of the reduced *Aae*Fd4 variants at pH ≈ 6.5 are characterized by the presence of two intense positive bands between 350 and 400 nm, a broad less-intense positive band around 670 nm, and an intense negative band at ∼ 470 nm (Figure 4). As the pH is increased, these bands shift and become less intense with the observation of one set of isosbestic points that indicates direct interconversion between low and high pH species. Plots of the CD intensity around 385 nm with increasing pH were used to determine the pK_a values and number of protons involved in the conversion between the low and high pH forms of both variants; see insets in Figure 4. The data were fit using eq 2, where A_{obs} is the observed CD intensity at a particular wavelength and where A_l and A_h are the CD intensities at this wavelength at low and high pH, respectively.

$$A_{obs} = \frac{(A_l - A_h)10^{-pH}}{(10^{-pH} + 10^{-pK_a})} + A_h \quad (2)$$

The results indicate a single protonation event with pK_a of approximately 9.0 and 8.3 for the reduced C55S and C59S variants, respectively. The significantly lower pK_a for the C59S

DOI: 10.1021/jacs.5b01869
J. Am. Chem. Soc. 2015, 137, 4567−4580

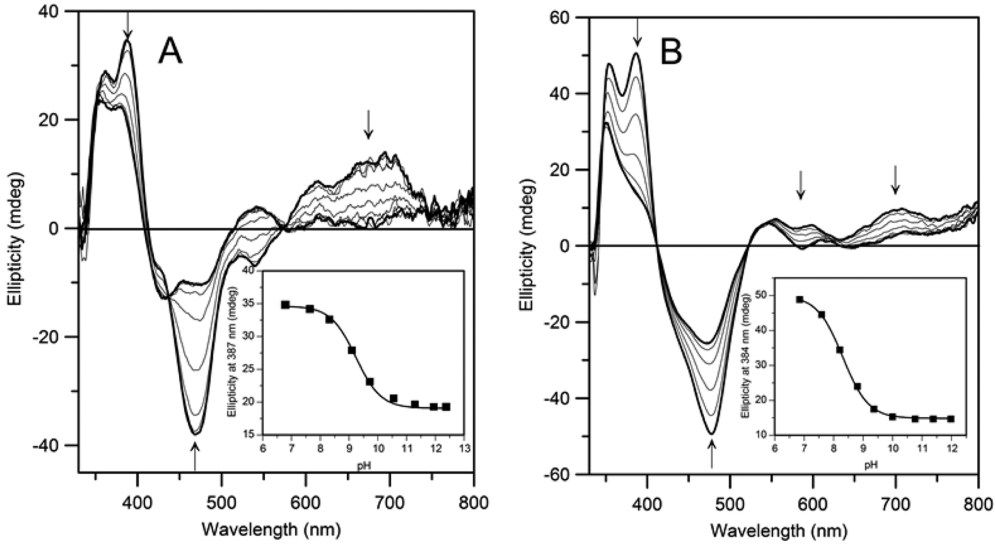

Figure 4. CD spectra of dithionite-reduced C55S *Aae*Fd4 (A) and C59S *Aae*Fd4 (B) measured as a function of pH. The titrations were carried out under anaerobic conditions in a 1.0 cm cuvette, using 0.09 mM dithionite-reduced C55S *Aae*Fd4 and 0.11 mM dithionite-reduced C59S *Aae*Fd4 in a mixed buffer system (50 mM Tris, 50 mM CHES, 50 mM CAPS, 50 mM phosphate, and 0.1 M NaCl), by adding aliquots of NaOH. Arrows indicate the direction of change in CD intensity at selected wavelengths with increasing pH. The insets show plots of the ellipticity at 387 nm (A) and 384 nm (B) versus pH, and the solid lines represent best fits to a single deprotonation event with pK_a values of 9.0 and 8.3 for dithionite-reduced C55S *Aae*Fd4 (A) and C59S *Aae*Fd4 (B), respectively.

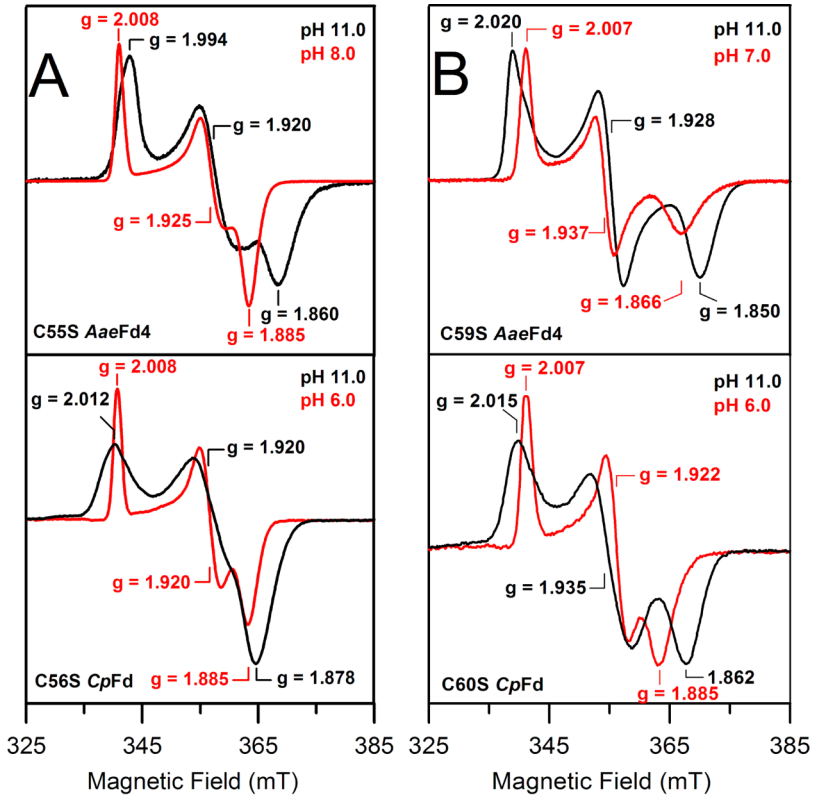

Figure 5. Comparisons of the X-band EPR spectra of dithionite-reduced C55S *Aae*Fd4 and C56S *Cp*Fd (A) and C59S *Aae*Fd4 and C60S *Cp*Fd (B) in the $S = 1/2$ region at pH values at least 1 unit above and below the pK_a values. The spectra were recorded at 35 K with a microwave frequency of 9.58 GHz, modulation amplitude of 0.64 mT, and a microwave power of 0.5 mW.

variant provides rationalization for the significantly lower midpoint potential that is observed at pH 7 for the C59S variant (−420 mV) compared to the C55S variant (−380 mV) (Table 1). Hence the pH-dependent redox properties of the WT and variant forms of *Aae*Fd4 and *Cp*Fd are clearly very similar except for a lower pK_a for protonation of reduced C59S *Aae*Fd4.

Since high resolution crystallographic studies have provided definitive evidence for serinate cluster ligation in the C55S and C59S variants of oxidized *Aae*Fd4[13,21] and film voltammetry of the C56S and C60S variants of *Cp*Fd showed sharp and

DOI: 10.1021/jacs.5b01869
J. Am. Chem. Soc. 2015, 137, 4567−4580

symmetrical oxidation and reduction waves at pH > 10 (see Figures S2 and S3), we conclude that serinate cluster ligation is retained at pH > 10 on reduction of the $[Fe_2S_2]^{2+,+}$ centers in both the *Aae*Fd4 and *Cp*Fd variants. The protonation event with pK_a values between 8.3 and 9.0 is therefore attributed to protonation of the serine ligand. As protonated serine is expected to be a weak cluster ligand and the reducible Fe site of the cluster is solvent exposed based on crystallographic studies of *Aae*Fd4 variants,[13] it seems likely that serine is replaced as a ligand by water or hydroxide when samples are reduced at pH values below the pK_a. Such coupling to a ligand exchange reaction is the likely cause of the broader and more asymmetrical voltammetric waves that are observed at lower pH values (see Figures S2 and S3).

EPR Studies. The ground state properties of the $[Fe_2S_2]^+$ clusters in the *Aae*Fd4 and *Cp*Fd variants at low and high pH were investigated by EPR and VHVT MCD saturation magnetization studies. WT samples of dithionite-reduced *Aae*Fd4 and *Cp*Fd exhibit almost identical rhombic $S = 1/2$ EPR signals ($g \approx 2.00, 1.95, 1.92$; $g_{av} \approx 1.96$) accounting for 1.0 ± 0.1 spin/cluster[15,19] that are invariant to pH over the pH range 6−11. Comparisons of the X-band EPR spectra of anaerobically prepared, dithionite-reduced samples of the Cys-to-Ser variants *Aae*Fd4 and *Cp*Fd in the $S = 1/2$ region at pH values significantly above and below the observed pK_a values are shown in Figure 5. Compared to WT, the *g*-value anisotropy increases and the average *g*-value decreases (g_{av} = 1.925−1.938) for each of the Cys-to-Ser variants, as expected for replacing a cysteinate ligand with an oxygenic ligand at the reducible Fe site.[20,22−24] In addition, distinct $S = 1/2$ EPR signals are observed at low and high pH values, with the high pH samples invariably exhibiting greater *g*-value anisotropy, suggesting distinct types of oxygenic ligands at low and high pH. Spin quantitations indicate that the $[Fe_2S_2]^+$ clusters have exclusively $S = 1/2$ ground states for the low pH samples of the reduced *Cp*Fd and *Aae*Fd4 variants. However, spin quantitations at pH 11.0 indicate that the $S = 1/2$ resonances accounted for 0.90 ± 0.07 spin/cluster for the *Aae*Fd4 variants and 0.50 ± 0.05 spin/cluster for the *Cp*Fd variants. As shown below, the substoichiometric $S = 1/2$ spin quantitations are a consequence of some of the $[Fe_2S_2]^+$ clusters having $S = 9/2$ ground states.

Previous EPR studies of dithionite-reduced C56S and C60S *Cp*Fd at pH 11.0 at temperatures between 4.2 and 60 K revealed low-field resonances from $[Fe_2S_2]^+$ clusters with $S = 9/2$ ground states ($E/D = 0.12$, $D < 0$, $g_0 = 2.00$ for C56S and $E/D = 0.16$, $D < 0$, $g_0 = 2.04$ for C60S).[5,8] These resonances were attributed to valence-delocalized $[Fe_2S_2]^+$ clusters, an interpretation that was subsequently confirmed by Mössbauer spectroscopy.[9] Very similar resonances with analogous temperature-dependent behavior, albeit with much lower intensity, were also observed in the low-field region of the dithionite-reduced C55S and C59S *Aae*Fd4 samples at pH 11.0; see Figure 6. The effective *g*-values and the observed temperature dependence for the low-field components are readily interpreted in terms of a conventional $S = 9/2$ spin Hamiltonian with $E/D = 0.12$, $D < 0$, and $g_0 = 2.00$ for the C55S variant and $E/D = 0.175$, $D < 0$, and $g_0 = 2.04$ for the C59S variant (Table 2). The observation of $S = 9/2$ EPR signals at pH values significantly higher than the pK_a values of the reduced *Aae*Fd4 and *Cp*Fd variants is therefore interpreted in terms of serinate cluster ligation and the consequent changes in cluster redox properties. It also seems likely that the changes in the excited state electronic properties of the reduced clusters

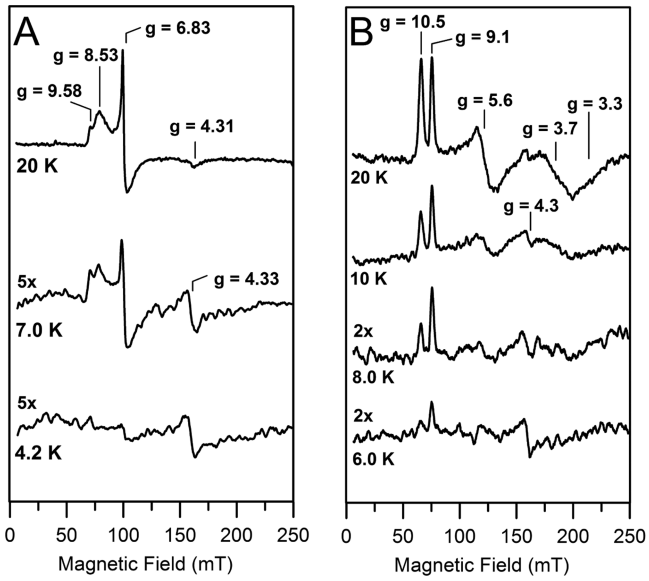

Figure 6. X-band EPR spectra in the low-field region for dithionite-reduced C55S *Aae*Fd4 (A) and C59S *Aae*Fd4 (B) at pH 11.0. The spectra were recorded at the indicated temperatures and a microwave frequency of 9.58 GHz, with modulation amplitude of 0.64 mT and a microwave power of 50 mW. Best fit spin Hamiltonian parameters that account for the observed effective *g*-values are shown in Table 2. The weak derivative resonance at $g = 4.33$ arises from adventitiously bound Fe^{3+}.

in the Cys-to-Ser variants as a function of pH, as revealed by room temperature absorption spectra, reflect the changes in spin state of the reduced cluster. Since VTMCD spectroscopy provides a more discriminating method for elucidating electronic excited state properties of paramagnetic chromophores, as well as means of assessing ground state properties via the analysis of VHVT MCD saturation magnetization data at discrete wavelengths, MCD studies were employed to further investigate the change in the spin-state and electronic excited state properties as a function of pH.

VTMCD Studies. The VTMCD spectra of the C55S and C59S variants of *Aae*Fd4 (Figure 7) surprisingly showed features characteristic of pure valence-localized $S = 1/2$ $[Fe_2S_2]^+$ clusters at both low and high pH.[25,26] Moreover, VHVT MCD saturation magnetization data at discrete wavelengths showed that all the observed MCD bands originate from $[Fe_2S_2]^+$ clusters with $S = 1/2$ ground states and provided no evidence for contributions from the valence-delocalized $S = 9/2$ $[Fe_2S_2]^+$ clusters that were observed by EPR. Parallel EPR studies indicated the addition of 50% (v/v) ethylene glycol to obtain a frozen glass for VTMCD studies results in complete loss of the EPR signals associated with the $S = 9/2$ $[Fe_2S_2]^+$ clusters. The VTMCD spectra of each variant are similar at pH 11 and 7, but parallel EPR spectra of the samples used for VTMCD studies demonstrated that 50% (v/v) ethylene glycol does not perturb the ground state properties of the high- and low-pH valence-localized $S = 1/2$ $[Fe_2S_2]^+$ clusters as judged by EPR spectra identical to those shown in Figure 5. We therefore conclude that 50% (v/v) ethylene glycol does not significantly alter the pK_a for serinate protonation but does perturb the environment of the solvent-exposed reducible Fe site of the $[Fe_2S_2]$ cluster, thereby preventing the formation of any valence-delocalized $S = 9/2$ $[Fe_2S_2]^+$ clusters in frozen solution.

DOI: 10.1021/jacs.5b01869
J. Am. Chem. Soc. 2015, 137, 4567−4580

Table 2. Effective *g*-Values and Spin Hamiltonian Parameters for the $S = 9/2$ $[Fe_2S_2]^+$ Centers in the Reduced C55A and C59S Variants of *Aae*Fd4[a]

C55S *Aae*Fd4, $E/D = 0.12$, $D < 0$, and $g_0 = 2.00$				C59S *Aae*Fd4, $E/D = 0.175$, $D < 0$, and $g_0 = 2.04$			
$\pm M_S\rangle$	g_x	g_y	g_z	$\pm M_S\rangle$	g_x	g_y	g_z
$\pm 1/2\rangle$	0.63	16.86	1.36	$\pm 1/2\rangle$	0.32	17.72	0.58
$\pm 3/2\rangle$	4.23 (4.31)	8.51 (8.53)	6.62 (6.83)	$\pm 3/2\rangle$	3.43 (~3.3)	10.51 (10.5)	5.62 (5.6)
$\pm 5/2\rangle$	9.52 (9.58)	1.72	1.94	$\pm 5/2\rangle$	9.05 (9.1)	3.21 (~3.3)	3.73 (3.7)
$\pm 7/2\rangle$	13.90	0.07	0.08	$\pm 7/2\rangle$	14.05	0.22	0.26
$\pm 9/2\rangle$	17.98	0.00	0.00	$\pm 9/2\rangle$	18.31	0.00	0.00

[a]Observed *g*-values are in parentheses.

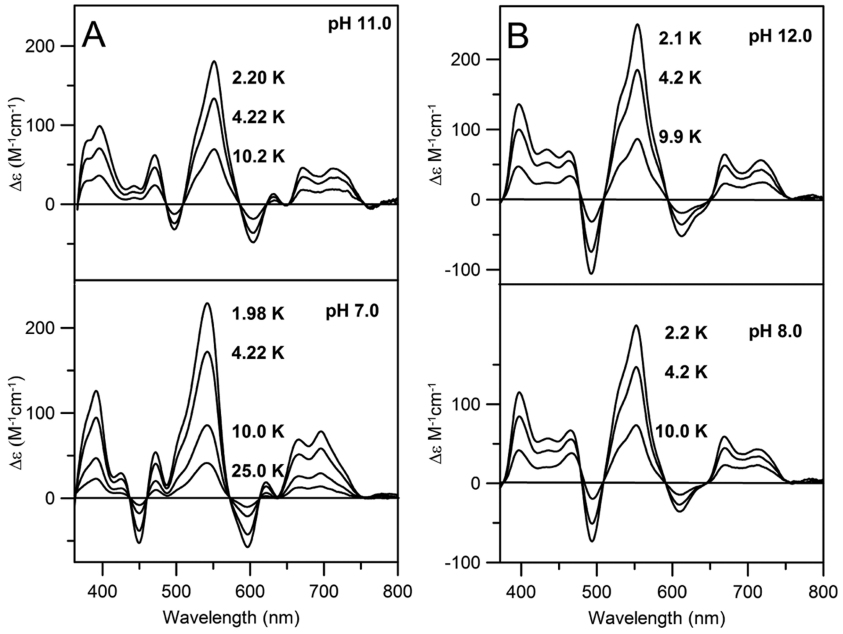

Figure 7. VTMCD spectra for the dithionite-reduced C55S and C59S *Aae*Fd4. (A) C55S *Aae*Fd4 (0.3 mM) at pH 7.0 in 200 mM Tris-HCl and at pH 11.0 in 200 mM CAPS buffer. (B) C59S *Aae*Fd4 (0.6 mM) at pH 7.0 in 200 mM Tris-HCl and at pH 12.0 in 200 mM CAPS buffer. All samples contained 50% (v/v) ethylene glycol, and the spectra were recorded with a magnetic field of 6.0 T. MCD intensity increases with decreasing temperature for all samples.

Unlike the *Aae*Fd4 variants, the VTMCD spectra of the dithionite-reduced *Cp*Fd C56S and C60S variants are quite different at low and high pH; see Figure 8. At low pH, the MCD bands are characteristic of valence-localized $S = 1/2$ $[Fe_2S_2]^+$ clusters, and the VTMCD spectra are very similar to those of the corresponding *Aae*Fd4 variants. However, the VTMCD spectra of the dithionite-reduced C56S and C60S samples are both markedly different at high pH compared to low pH, and both exhibit very different temperature dependence behavior for individual bands that suggests a mixture of $S = 1/2$ and $9/2$ $[Fe_2S_2]^+$ clusters, in accord with parallel EPR studies of the VTMCD samples. In contrast to the reduced *Aae*Fd4 variants, quantitative EPR studies of the *Cp*Fd variants indicated an approximate 50:50 mixture of $S = 1/2$ and $9/2$ $[Fe_2S_2]^+$ centers that was not significantly perturbed by the addition of 50% (v/v) ethylene glycol, but the MCD spectra are clearly dominated by the $S = 9/2$ component based on the temperature dependence behavior of individual bands. Since the $S = 9/2$ $[Fe_2S_2]^+$ centers approach magnetic saturation much more rapidly than the $S = 1/2$ $[Fe_2S_2]^+$ centers with decreasing temperature at 6 T, the VTMCD spectra of the $S = 9/2$ centers dominate at ~50 K. Hence the $S = 9/2$ $[Fe_2S_2]^+$ centers in the C56S and C60S variants have very similar VTMCD spectra (intense positive bands centered near 470 and 710 nm, weak positive bands centered near 900 and 1070 nm, and strong negative bands centered near 330 and 600 nm) that are quite distinct from the VTMCD spectra of the $S = 1/2$ $[Fe_2S_2]^+$ centers, indicating very different excited state electronic properties for the $S = 1/2$ and $9/2$ $[Fe_2S_2]^+$ centers. Notably the valence-delocalized $S = 9/2$ $[Fe_2S_2]^+$ centers have distinctive bands in the low energy 600−1400 nm region that are not present in valence-delocalized $S = 1/2$ $[Fe_2S_2]^+$ centers; see Figure 8.

VHVT MCD magnetization studies were used to investigate the ground-state properties and excited-state transition polarizations of the $S = 9/2$ $[Fe_2S_2]^+$ centers in high-pH, dithionite-reduced C56S and C60S *Cp*Fd; see Figure 9. The data obtained by varying the magnetic field (0−6 T) at three fixed temperatures (1.64, 4.22, and 10.0 K) were fit based on the EPR-determined spin Hamiltonian parameters ($D < 0$ and $E/D = 0.12$ for C56S; and $D < 0$ and $E/D = 0.16$ for C60S) and using D and the transition dipole moments in the *xy*, *xz*, and *yz* planes (M_{xy}, M_{xz}, and M_{yz}) as variable parameters using the methodology developed by Neese and Solomon.[18] Satisfactory theoretical fits for the VHVT MCD magnetization data collected at ~710 nm required a small contribution from $S = 1/2$ $[Fe_2S_2]^+$ centers (15% for C56S and 10% for C60S). For both variants, the dominant $S = 9/2$ components near 710 nm

DOI: 10.1021/jacs.5b01869
J. Am. Chem. Soc. 2015, 137, 4567−4580

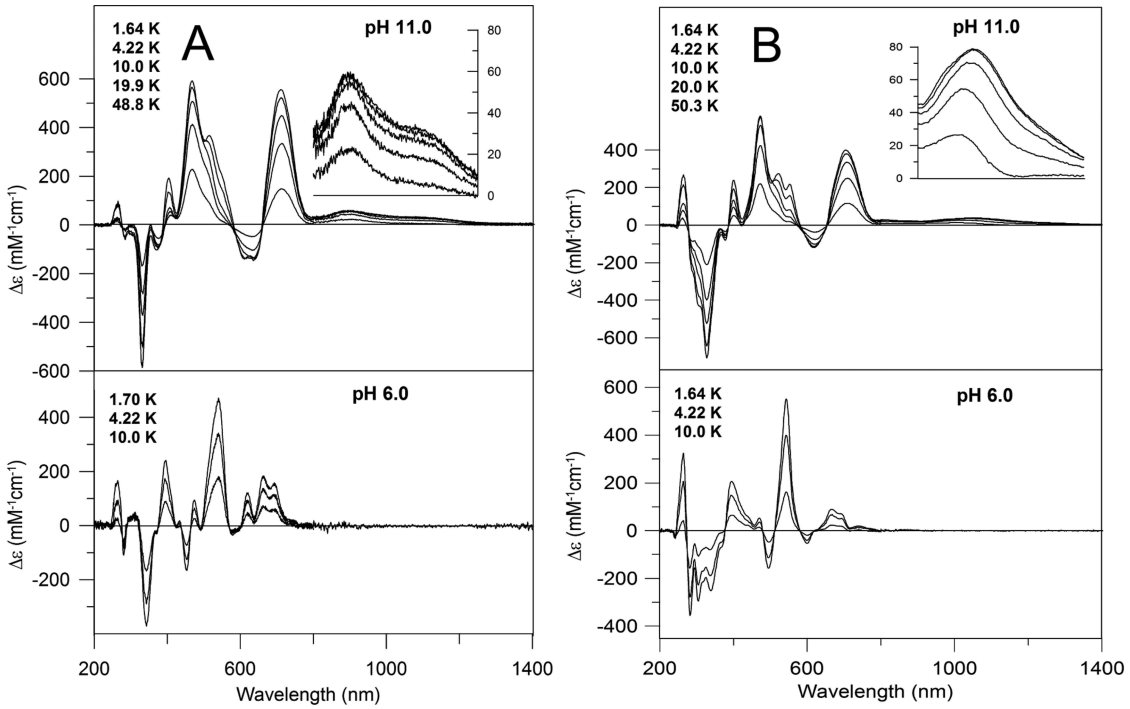

Figure 8. UV−visible−NIR VTMCD spectra of dithionite-reduced C56S and C60S *Cp*Fd. (A) C56S *Cp*Fd at pH 6.0 (0.72 mM in 100 mM MES buffer) and pH 11.0 (0.21 mM in 100 mM CAPS buffer). (B) C60S *Cp*Fd at pH 6.0 (0.82 mM in 100 mM MES buffer) and pH 11.0 (0.20 mM in 100 mM CAPS buffer). All samples contained 50% (v/v) ethylene glycol, and the spectra were recorded in 0.1 cm cuvettes at a magnetic field of 6.0 T at the temperature indicated on the spectra. MCD intensity increases with decreasing temperature for all samples.

were best fit as predominantly *xz*-polarized transitions with significant contributions for both *xy*- and *yz*-polarized transitions (M_{xy}:M_{xz}:M_{yz} = +0.70:+1.00:−0.70 for C56S at 712 nm; M_{xy}:M_{xz}:M_{yz} = +0.67:+1.00:−0.67 for C60S at 705 nm) with $D = -1.5 \pm 0.4$ cm^{-1} and -1.4 ± 0.3 cm^{-1} for C56S and C60S, respectively, see Figure 9A and Figure 9D. The same axial zero field parameters, D, were used in fitting the weak bands in the NIR region which arise exclusively from an S = 9/2 ground state but exhibit very different VHVT MCD magnetization data. Only the C56S variant exhibited a well resolved band at 895 nm, and fits of the VHVT MCD magnetization data indicate a uniaxial *y*-polarized transition (M_{xy}:M_{xz}:M_{yz} = +1.00:+0.05:+1.00); see Figure 9C. Both variants exhibit bands centered at ∼1070 nm, and these transitions were shown to be almost exclusively *z*-polarized (M_{xy}:M_{xz}:M_{yz} = +0.15:−1.00:+0.69 for C56S which corresponds to 93% *z*-polarized; M_{xy}:M_{xz}:M_{yz} = +0.15:−1.00:+0.55 for C60S which corresponds to 91% *z*-polarized); see Figure 9B and Figure 9E. The low intensity of the observed uniaxial VTMCD transitions is expected as MCD *C*-term intensity formally requires two nonzero perpendicular transition moments. The observation of a low energy *z*-polarized transition for a valence-delocalized S = 9/2 $[Fe_2S_2]^+$ center is particularly important, as it is an excellent candidate for the $\sigma \rightarrow \sigma^*$ transition associated with the Fe−Fe interaction.

Medium Effects on the Spin-State Heterogeneity. The results of EPR and VTMCD studies on the Cys-to-Ser variants in *Aae*Fd4 and *Cp*Fd summarized thus far indicate that the $[Fe_2S_2]^+$ centers in these variants can exist in two different spin states at high pH in frozen solutions: valence-localized S = 1/2 and valence-delocalized S = 9/2. EPR spin quantitations indicate that approximately 10% and 50% of the reduced clusters are present in the S = 9/2 state in reduced high-pH *Aae*Fd4 and *Cp*Fd variants, respectively. Since one of the objectives of this work was to find conditions conducive to obtaining samples of reduced *Aae*Fd4 variants with homogeneous valence-delocalized S = 9/2 $[Fe_2S_2]^+$ centers in order to facilitate structural characterization of the determinants of spin-dependent resonance delocalization, we investigated the effects of the medium and freezing rate on the spin-state heterogeneity using EPR spectroscopy. To investigate the possibility that the rate of freezing affects the extent of valence delocalization, EPR samples of the reduced C55S *Aae*Fd4 at pH 11.0/12.0 were prepared by rapid freezing in an isopentane bath using an Update freeze quench apparatus and slow freezing in liquid nitrogen. However, the rate of freezing did not affect the extent of valence localization as EPR spin quantitations revealed that 90% of the clusters remained in the valence localized S = 1/2 form. To investigate buffer effects and the possibility of apparent pH changes upon freezing, samples at high pH were also prepared in phosphate and mixed buffers. However, the samples revealed no difference in the spin-state heterogeneity as determined by quantitative EPR studies. Samples were also prepared in mixed buffers at different ionic strengths by varying the salt concentration (0.025−0.5 M NaCl), but again no significant change in spin-state heterogeneity was apparent.

Since the addition of ethylene glycol to the *Aae*Fd4 variants at high pH for VTMCD studies resulted in the observation of 100% valence-localized S = 1/2 $[Fe_2S_2]^+$ clusters, different glassing agents were used to perturb the solvent medium around the solvent exposed Fe site, in an attempt to promote the observation of valence-delocalized S = 9/2 state. However, neither the addition of 50% (v/v) glycerol nor polyethylene glycol as the glassing agent was successful in mediating a change in the spin state of the $[Fe_2S_2]^+$ center, which remained in the valence-localized S = 1/2 state. Variable-temperature

DOI: 10.1021/jacs.5b01869
J. Am. Chem. Soc. 2015, 137, 4567−4580

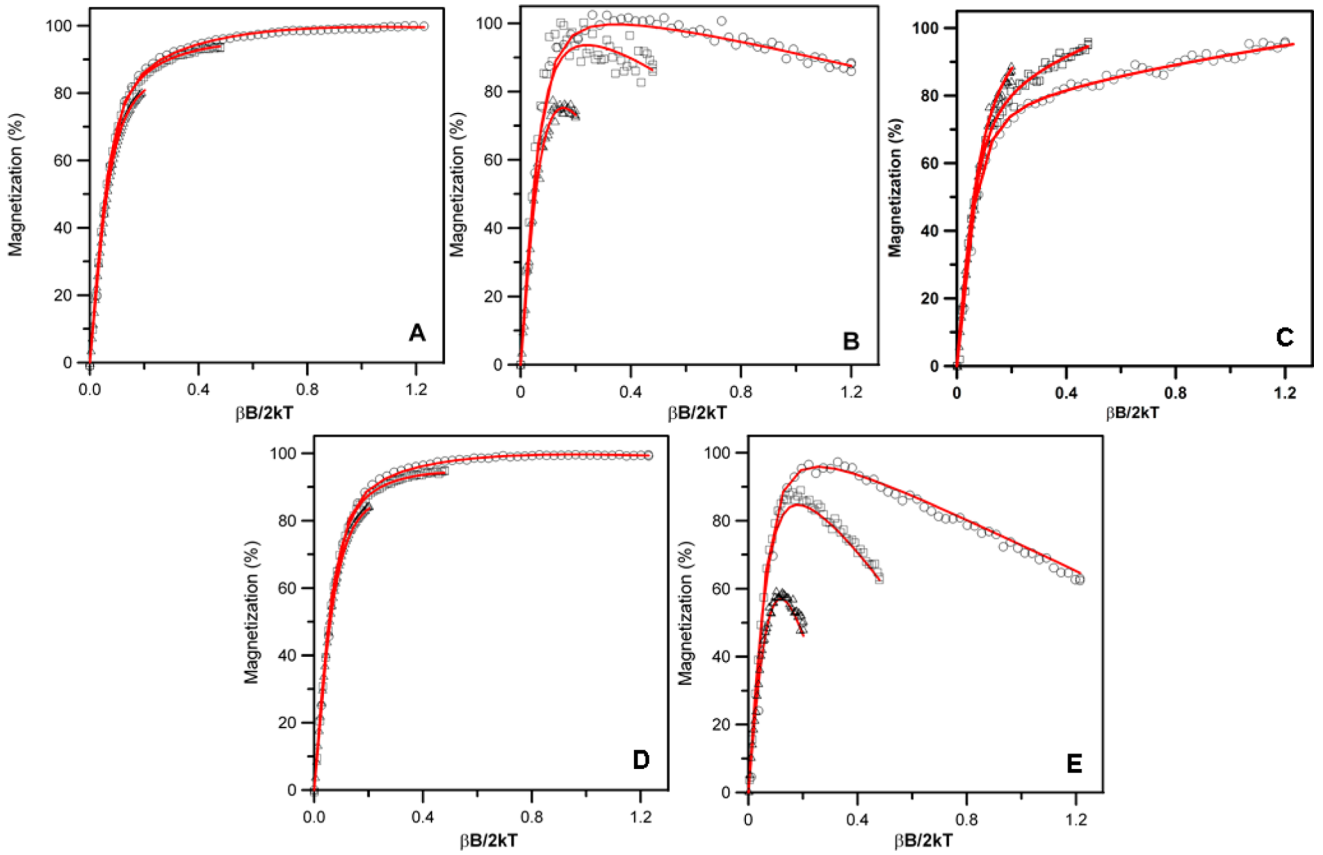

Figure 9. VHVT MCD magnetization data for dithionite-reduced C56S and C60S *Cp*Fd at pH 11.0. Samples are as described in the figure. MCD magnetization data were collected at temperatures of 1.64 K (○), 4.22 K (□), and 10.0 K (△) with magnetic fields in the range 0−6 T. (A) C56S *Cp*Fd at 712 nm. Solid red line corresponds to theoretical VHVT MCD magnetization data for 85% of a predominantly *xz*-polarized transition (M_{xy}:M_{xz}:M_{yz} = +0.70:+1.00:−0.70) from a S = 9/2 ground state with D = −1.5 cm^{-1} and E/D = 0.12 and 15% of an S = 1/2 ground state with g = 2.01, 1.92, and 1.88. (B) C56S *Cp*Fd at 1070 nm. Solid red line corresponds to theoretical VHVT MCD magnetization data for a predominantly (93%) *z*-polarized transition (M_{xy}:M_{xz}:M_{yz} = +0.15:−1.00:+0.69) from a S = 9/2 ground state with D = −1.5 cm^{-1} and E/D = 0.12. (C) C56S *Cp*Fd at 895 nm. Solid red line corresponds to theoretical VHVT MCD magnetization data for a uniaxial *y*-polarized transition (M_{xy}:M_{xz}:M_{yz} = +1.00:+0.05:+1.00) from a S = 9/2 ground state with D = −1.5 cm^{-1} and E/D = 0.12. (D) C60S *Cp*Fd at 705 nm. Solid red line corresponds to theoretical VHVT MCD magnetization data for 90% of a predominantly *xz*-polarized transition (M_{xy}:M_{xz}:M_{yz} = +0.67:+1.00:−0.67) from a S = 9/2 ground state with D = −1.4 cm^{-1} and E/D = 0.16 and 10% of an S = 1/2 ground state with g = 2.02, 1.94, and 1.86. (E) C60S *Cp*Fd at 1070 nm. Solid lines correspond to theoretical VHVT MCD magnetization data for a predominantly (91%) *z*-polarized transition (M_{xy}:M_{xz}:M_{yz} = +0.15:−1.00:+0.55) from a S = 9/2 ground state with D = −1.4 cm^{-1} and E/D = 0.17.

Mössbauer studies on C56S *Cp*Fd indicated an increase in the fraction of valence-delocalized $[Fe_2S_2]^+$ clusters from 50% at 4.2 K to ∼94% at 200 K with a transition temperature of about 100 K. Moreover, high temperature magnetic susceptibility data on frozen samples (80−200 K) convincingly demonstrated that this was not accompanied by a S = 1/2 to 9/2 transition. Rather, this was attributed to a rapid increase in the electron transfer (ET) rates between the two iron sites resulting in a valence-delocalized S = 1/2 $[Fe_2S_2]^+$ cluster on the Mössbauer time scale (∼10^{-7} s), i.e., $\tau_{ET} > \tau_{Mössbauer}$.[10] To investigate if such a transition is observable for the *Aae*Fd4 variants on the time scale of electronic transitions (10^{-14}−10^{-16} s), the VTMCD spectra of the C55S *Aae*Fd4 variant at pH 11.0 were recorded at 2.0, 4.2, 10, 50, 100, and 230 K. The MCD spectrum associated with the valence-localized S = 1/2 $[Fe_2S_2]^+$ cluster remained unchanged up to 230 K, indicating that valences remain localized on the electronic transition time scale with increasing temperature.

RTMCD Studies. The observation that the dramatic changes in the room-temperature UV−visible absorption spectra for the low and high pH forms of the *Cp*Fd and *Aae*Fd4 variants appear to mirror the changes in the electronic transitions for the S = 1/2 valence-localized and S = 9/2 valence-delocalized $[Fe_2S_2]^+$ centers as judged by VTMCD spectroscopy raised the possibility that the high pH samples are S = 9/2 valence-delocalized at room temperature and only become valence-localized S = 1/2 on freezing samples for EPR, VTMCD, and Mössbauer studies. To investigate this hypothesis, the RTMCD spectra of the high and low pH samples of the reduced *Aae*Fd4 and *Cp*Fd variants were measured and compared with each other and the better resolved low-temperature MCD spectra of the S = 1/2 valence-localized and S = 9/2 valence-delocalized $[Fe_2S_2]^+$ centers in frozen solution. The RTMCD spectra of the reduced *Aae*Fd4 and the *Cp*Fd variants at low pH (Figure 10) are both very similar to those of the valence-localized S = 1/2 $[Fe_2S_2]^+$ cluster in frozen solution as determined by VTMCD, with positive bands centered around 400, 540, and 690 nm and a negative band around 460 nm. However, at high pH, unlike the low-temperature MCD data for the *Aae*Fd4 variants, the spectra are characteristic of a valence-delocalized S = 9/2 $[Fe_2S_2]^+$ cluster (Figure 10). The complete absence of the positive band

DOI: 10.1021/jacs.5b01869
J. Am. Chem. Soc. 2015, 137, 4567−4580

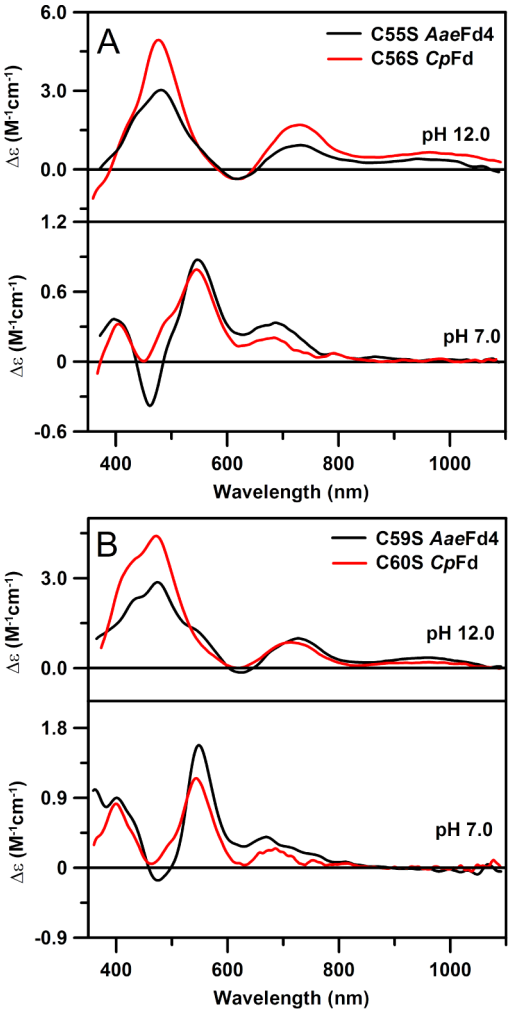

Figure 10. (A) Comparison of the RTMCD spectra of C55S *Aae*Fd4 and C56S *Cp*Fd at pH 7.0 and 12.0. (B) Comparison of the RTMCD spectra of C59S *Aae*Fd4 and C60S *Cp*Fd at pH 7.0 and 12.0. All MCD spectra were recorded using an applied magnetic field of 1.5 T. The samples (0.5−1.0 mM in $[Fe_2S_2]$ clusters) were prepared in 200 mM mixed buffer with 0.1 M NaCl, and the pH was adjusted to 7.0 or 12.0.

centered around 540 nm, and the presence of positive bands centered at 480, 720, and ∼1000 nm and a negative band centered at 600 nm unambiguously identifies the excited state electronic structure of valence-delocalized $S = 9/2$ $[Fe_2S_2]^+$ clusters in the high pH samples at room temperature. Hence, on electronic time scale, we conclude that valence localization of the high pH variants occurs on freezing samples for spectroscopic studies and that high pH samples of both the *Aae*Fd4 and *Cp*Fd variants are predominantly or exclusively valence-delocalized with $S = 9/2$ ground states at room temperature.

DISCUSSION

The thioredoxin class of $[Fe_2S_2]$ ferredoxins, typified by *Cp*Fd, is unique in providing the only known examples of biological or synthetic valence-delocalized $[Fe_2S_2]^+$ centers. The objectives of this work were to compare the detailed spectroscopic and redox properties of the $[Fe_2S_2]$ centers in the highly homologous *Cp*Fd and *Aae*Fd4 proteins with a view toward characterizing valence-delocalized $[Fe_2S_2]^+$ centers in the structurally characterized Cys-to-Ser variants of *Aae*Fd4,[13] thereby addressing the origins of valence delocalization in Fe−S clusters. Valence-delocalized $S = 9/2$ $[Fe_2S_2]^+$ fragments are integral constituents of all biological and synthetic Fe−S clusters containing three or more Fe atoms.[4,6] However, valence-delocalized $S = 9/2$ $[Fe_2S_2]^+$ clusters have thus far only been observed in C56S and C60S variants of *Cp*Fd, where the reduced clusters were found to be present as mixtures of $S = 9/2$ valence-delocalized and $S = 1/2$ valence-localized forms in frozen solution.[5,8−10] The spectroscopic results presented in this work demonstrate that the $[Fe_2S_2]^+$ clusters in the reduced forms of C56S and C60S *Cp*Fd and C55S and C59S *Aae*Fd4 are predominantly or exclusively present as $S = 9/2$ valence delocalized centers at pH ≥ 10 in aqueous solution at room temperature. However, in all four variants the reduced clusters revert completely or partially to $S = 1/2$ valence-localized centers upon freezing samples for spectroscopic studies. Nevertheless, the equivalent variants of *Cp*Fd and *Aae*Fd4 are shown to have almost identical $S = 9/2$ valence delocalized $[Fe_2S_2]^+$ centers and the significant concentrations of $S = 9/2$ valence delocalized $[Fe_2S_2]^+$ centers that are present in the

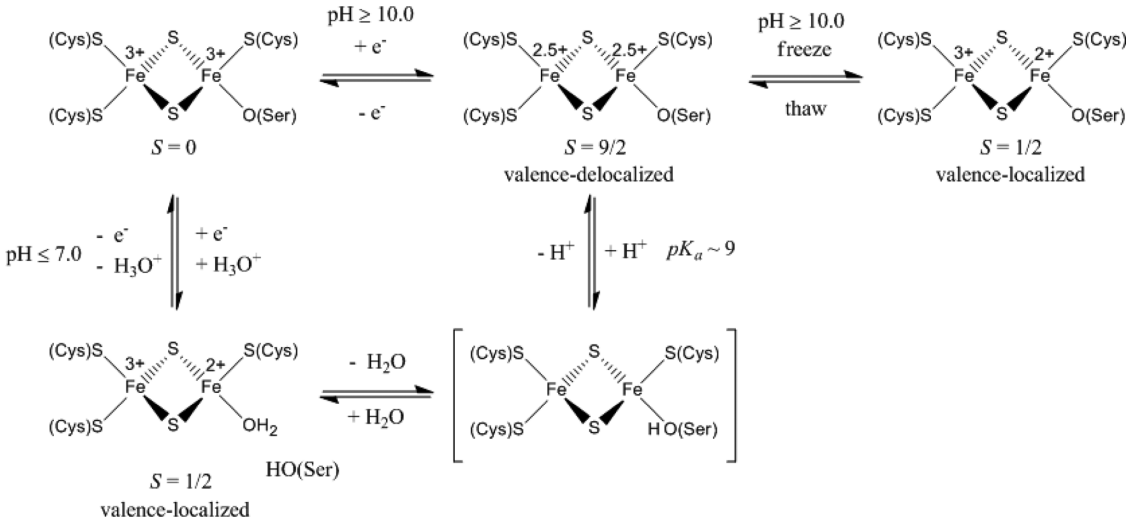

Figure 11. Schematic summary of the proposed ligation, spin states, and redox properties of the $[Fe_2S_2]^{2+,+}$ centers in the Cys-to-Ser variants of *Cp*Fd and *Aae*Fd4 as a function of pH.

DOI: 10.1021/jacs.5b01869
J. Am. Chem. Soc. 2015, 137, 4567−4580

frozen samples of reduced C56S and C60S *Cp*Fd have facilitated detailed characterization of the ground and excited state electronic properties of these novel species using VTMCD and EPR spectroscopies.

The scheme in Figure 11 summarizes the ligation, spin states, and redox properties of the $[Fe_2S_2]^{2+,+}$ centers in the Cys-to-Ser variants of *Cp*Fd and *Aae*Fd4 as a function of pH, based on the high resolution structural studies of oxidized C55S and C59S *Aae*Fd4[13] and the spectroscopic and redox studies of C56S and C60S *Cp*Fd and C55S and C59S *Aae*Fd4 reported in this work. Crystallographic data collected at 77 K provide direct evidence for serinate ligation at the solvent-exposed reducible Fe site of the $S = 0$ antiferromagnetically coupled $[Fe_2S_2]^{2+}$ centers in oxidized C55S and C59S *Aae*Fd4.[13] Moreover, the absence of any changes in the UV−visible absorption and CD spectra of the oxidized proteins as a function of pH in the range pH 6−11 indicates that serinate remains a ligand to the oxidized cluster at high and low pH. In contrast, the reduced clusters of all four variant proteins undergo protonation equilibria with pK_a values between 8.3 and 9.0, which appear to involve the serinate ligand as protonation induces marked changes in the UV−visible absorption and CD properties of the reduced clusters in the Cys-to-Ser variant ferredoxin but not in the WT ferredoxin. At pH values at least 1 unit above the pK_a, serinate remains as a ligand to the reduced cluster, as evidenced by sharp and symmetrical oxidation and reduction waves in cyclic voltammograms. The resultant high-pH reduced $[Fe_2S_2]^+$ cluster is proposed to be valence delocalized with a $S = 9/2$ ground state at room temperature, based on comparison of the RTMCD with the low temperature MCD of the $S = 9/2$ valence-delocalized $[Fe_2S_2]^+$ centers in high pH samples of reduced C56S and C60S *Cp*Fd in frozen solution. However, the combination of EPR and VTMCD studies demonstrate that the $[Fe_2S_2]^+$ centers are completely or partially converted to a serinate-ligated, valence-localized $S = 1/2$ form on freezing high pH samples for spectroscopic investigation. For each variant, lowering the pH of reduced samples well below the pK_a or reducing oxidized samples at pH values well below the pK_a of the reduced samples results in a valence-localized $S = 1/2$ $[Fe_2S_2]^+$ center with EPR spectra that are distinct from the corresponding high-pH valence-localized $S = 1/2$ $[Fe_2S_2]^+$ center. The solvent-exposed nature of the reducible Fe site in the mutant proteins that results in water-to-serinate O_γ hydrogen bonds,[13] coupled with the observation of unsymmetrical oxidative and reductive waves in the cyclic voltammograms at low pH, therefore suggests that the serinate ligand is protonated and replaced by a H_2O or OH^- ligand in the low-pH valence-localized $S = 1/2$ $[Fe_2S_2]^+$ centers.

The spectroscopic and redox results for *Cp*Fd and *Aae*Fd4 clearly indicate that serinate ligation at the reducible Fe site is required to observe valence-delocalized $S = 9/2$ $[Fe_2S_2]^+$ centers in the thioredoxin-class of $[Fe_2S_2]$ Fds. However, detailed characterization of the ground and excited state properties of the valence-delocalized $S = 9/2$ $[Fe_2S_2]^+$ centers at high pH in the reduced *Aae*Fd4 Cys-to-Ser variants was not possible because of near quantitative conversion to valence-localized $S = 1/2$ $[Fe_2S_2]^+$ centers on freezing samples for EPR and VTMCD. Nevertheless, the electronic properties are expected to be very similar to those of the equivalent high-pH *Cp*Fd variants based on the close similarity in the observed EPR signals ($E/D = 0.12$ and $D < 0$ for both C56S *Cp*Fd and C55S *Aae*Fd4; $E/D = 0.16$ and $D < 0$ for C60S CpFd, and $E/D = 0.175$ and $D < 0$ for C59S *Aae*Fd4). Although $S = 9/2$ valence-delocalized and $S = 1/2$ valence-localized $[Fe_2S_2]^+$ centers are present in an approximately 50:50 mixture in frozen samples of reduced C56S and C60S *Cp*Fd at high pH, contributions from each to the VTMCD spectra can be deconvoluted based on dramatic differences in the temperature dependence of transitions originating from the $S = 9/2$ and $1/2$ ground states; see Figure 8. Moreover, by use of the EPR-determined ground state-spin Hamiltonian parameters, VHVT MCD saturation magnetization data can be used to assess the magnitude of the axial zero-field splitting parameter, D, and transition polarizations. The latter are particularly important for assigning low-energy transitions in the near-IR region that originate from the predominantly Fe-based MOs associated with the $Fe_2(\mu_2\text{-S})$ core and the Fe−Fe orbital overlap which is responsible for spin-dependent resonance delocalization.

A schematic diagram for the predominantly Fe-based MOs associated with a protein-bound valence-delocalized $S = 9/2$ $[Fe_2S_2]^+$ cluster is shown in Figure 12. The starting point

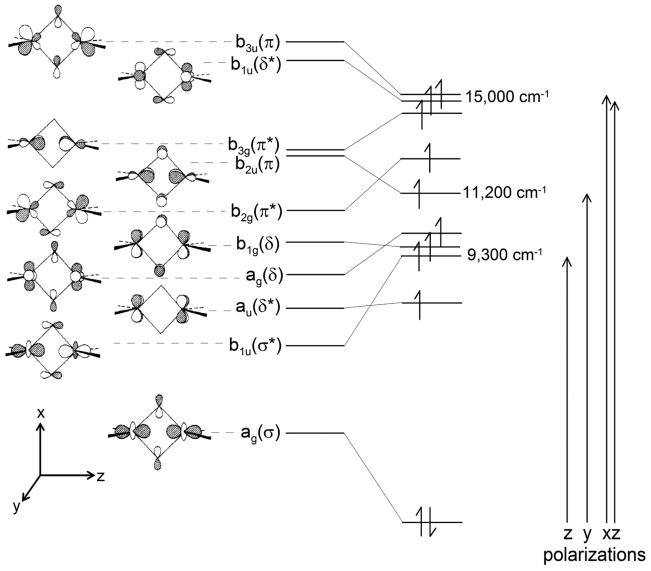

Figure 12. Schematic MO diagram with electronic assignments and transition polarizations for a valence-delocalized $S = 9/2$ $[Fe_2S_2]^+$ center. The left side shows the mainly Fe 3d frontier antibonding MOs for $[Fe_2S_2(SH)_4]^{2-}$ with energies based on previously published SCF-Xα-SW calculations using idealized D_{2h} symmetry.[27,28] The right side shows the effect of decreased sulfide-mediated exchange coupling and enhanced Fe−Fe interactions that together result in an $S = 9/2$ valance-delocalized $[Fe_2S_2]^+$ center and the energies and polarizations of electric-dipole allowed electronic transitions under idealized D_{2h} symmetry.

corresponds to previously published SCF-Xα-SW MO calculations under idealized D_{2h} symmetry for the mainly Fe 3d frontier antibonding MOs of the antiferromagnetically coupled $S = 0$ $[Fe_2S_2]^{2+}$ cluster in $[Fe_2S_2(SH)_4]^{2-}$.[27,28] Strong antiferromagnetic Heisenberg exchange interaction is mediated by the covalency of the bridging sulfides and results primarily in large splittings of the symmetric and antisymmetric d_{xz} (b_{2g} and b_{3u}) and $d_{x^2-y^2}$ (a_g and b_{1u}) pairs.[27,29] Valence delocalization leading to a ferromagnetic $S = 9/2$ $[Fe_2S_2]^+$ cluster requires increased Fe−Fe interactions which results in larger double exchange (B) and/or decreased Heisenberg exchange (J) such that $|B/J| > 9$. Although structures are not available for the high-pH, serinate-ligated reduced forms of the Cys-to-Ser variants of *Aae*Fd4, previous high-resolution structures of plant ferredoxins

DOI: 10.1021/jacs.5b01869
J. Am. Chem. Soc. 2015, 137, 4567−4580

showed no major structural reorganization on reduction.[30] Hence, the high-resolution crystallographic evidence for a 0.04 Å decrease in Fe−Fe distance in the serinate-ligated oxidized cluster compared to wild type[13] suggests enhanced Fe−Fe interactions in the serinate-ligated valence-delocalized reduced cluster. In Figure 12, the enhanced Fe−Fe interactions are manifest by a major increase in the σ overlap of d_{z^2} orbitals, i.e., increased separation between the symmetric and antisymmetric d_{z^2} pairs (a_g and b_{1u}), and a small increase in the π overlap for the d_{yz} orbitals, i.e., increased separation between the symmetric and antisymmetric d_{yz} pairs (b_{3g} and b_{2u}). Compared to $[Fe_2S_2(SH)_4]^{2-}$, decreased Heisenberg exchange for the $[Fe_2S_2]^+$ clusters in the mutant proteins is expected because of the asymmetry induced by serinate ligation[24] and the decreased covalency associated with two hydrogen-bonding interactions to each of the bridging sulfides.[13] In Figure 12, the decreased Heisenberg exchange interactions are manifest in decreased splittings of the symmetric and antisymmetric d_{xz} (b_{2g} and b_{3u}) and $d_{x^2-y^2}$ (a_g and b_{1u}) pairs. The resulting MOs rationalize the $S = 9/2$ ground state of the valence-delocalized $[Fe_2S_2]^+$ clusters in the Cys-to Ser variants of *Cp*Fd and *Aae*Fd4 in terms of a large energy separation between the fully occupied d_{z^2}−d_{z^2} σ-bonding MO and a set of nine closely spaced predominantly Fe 3d MOs. Moreover, as discussed below, the MO diagram facilitates quantitative rationalization of the number, polarizations, and energies of the low-energy VTMCD bands associated with the $S = 9/2$ valence-delocalized $[Fe_2S_2]^+$ cluster under idealized D_{2h} symmetry; see Figure 12.

VHVT MCD saturation magnetization data revealed that the low-energy temperature-dependent bands centered at 1070, 895, and 710 nm are primarily *z*-, *y*-, and *xz*-polarized, respectively. Uniaxial transitions are expected to give weak temperature-dependent MCD bands, since MCD *C*-term intensity requires two perpendicular nonzero transition dipole moments. Hence the weak *z*-polarized bands at ∼1070 nm (∼9300 cm^{-1}) in both variants are assigned to the $a_g \rightarrow b_{1u}$ ($\sigma \rightarrow \sigma^*$) transitions. Likewise the weak *y*-polarized band at 895 nm (11 200 cm^{-1}) in the C56S variant, which is less pronounced in the C60S variant, is assigned to the $a_g \rightarrow b_{2u}$ transition. The broad and intense "pseudo *A*-term" centered around 670 nm (15 000 cm^{-1}), with positive and negative bands at ∼710 and ∼630 nm, respectively, dominates the NIR region of the VTMCD spectrum and is attributed to a mainly *xz*-polarized band resulting from near-degenerate $a_g \rightarrow b_{1u}, b_{3u}$ transitions. The close proximity of the b_{3g} MO (which gives rise to a *y*-polarized transition under reduced C_{2v} symmetry) to the near degenerate b_{1u} and b_{3u} MOs is presumably responsible for the significant contributions from *xy*- and *yz*-polarized transitions. These NIR VTMCD bands appear to be the hallmark of $S = 9/2$ valence delocalized $[Fe_2S_2]^+$ centers, and the highest energy bands are readily observed in the NIR absorption spectra of high-pH dithionite-reduced samples as broad, poorly resolved bands centered near 630 and 710 nm; see Figures 1 and 2.

The importance of assigning the $\sigma \rightarrow \sigma^*$ transition is that the energy corresponds to $10B = 2\beta$, thereby providing direct assessment of the double exchange parameter (B) and thereby the resonance energy (β) associated with the spin-dependent resonance delocalization. Theoretical estimates of the value of B in $[Fe_2S_2]^+$ centers or fragments span a wide range from 30 to 1600 cm^{-1}.[7,24,31,32,32−37] On the basis of the VTMCD results reported herein, $B = 930 \pm 30$ cm^{-1} and $\beta = 4650 \pm 150$ cm^{-1} for the valence delocalized $S = 9/2$ $[Fe_2S_2]^+$ clusters C56S and C60S *Cp*Fd VT. However, these are likely to be underestimates due to mixing of the two b_{1u} MOs, which would lower the energy of the predominantly $\sigma \rightarrow \sigma^*$ transition. Indeed, these values are slightly below those estimated for a valence localized $[Fe_2S_2]^+$ cluster ($B = 965$ cm^{-1} and $\beta = 4825$ cm^{-1}), based on extrapolation from the Fe−Fe distance in a complex with a $[Fe_2(\mu_2\text{-}OH)_3]^{2+}$ core that is currently the best characterized example of a valence-delocalized $S = 9/2$ diiron complex.[29,38]

In addition, assignment of the transitions associated with the Fe−Fe interactions in the VTMCD spectra of valence-delocalized $S = 9/2$ $[Fe_2S_2]^+$ clusters provides a means of identifying and assigning analogous transitions associated with valence-delocalized $[Fe_2S_2]^+$ fragments in higher nuclearity clusters. This is illustrated in Figure 13 which compares the low

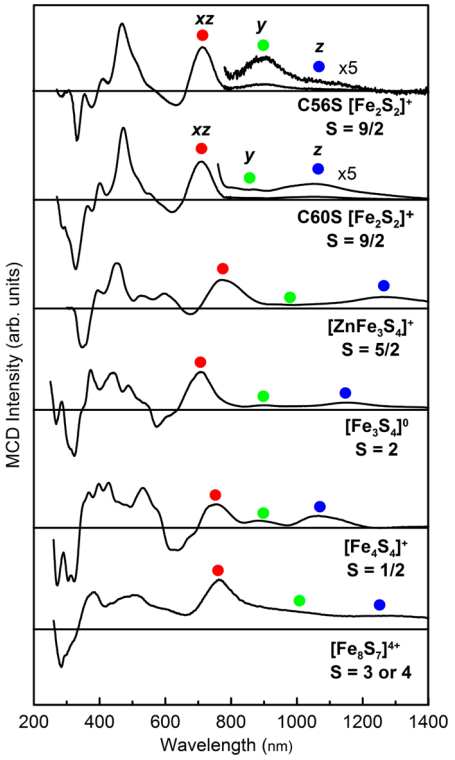

Figure 13. Comparison of the low temperature MCD spectra of the valence-delocalized $S = 9/2$ $[Fe_2S_2]^+$ center in high-pH reduced C56S and C60S *Cp*Fd with those of higher nuclearity Fe−S clusters believed to contain valence-delocalized $[Fe_2S_2]^+$ fragments. The 6 T and 50 K spectra are shown for C56S and C60S *Cp*Fd in order to emphasize the transitions from the $S = 9/2$ $[Fe_2S_2]^+$ component. All other spectra were recorded at 6 T and ∼1.6 K. The transition polarizations for the observed low energy transitions, as determined by VHVT MCD magnetization data, are shown for dithionite-reduced C56S and C60S *Cp*Fd.

temperature MCD spectrum of the valence-delocalized $S = 9/2$ $[Fe_2S_2]^+$ center in C56S and C60S *Cp*Fd with those of higher nuclearity clusters that are known to contain or have the potential to contain valence-delocalized $[Fe_2S_2]^+$ fragments, i.e., $S = 5/2$ $[ZnFe_3S_4]^+$ (which contains a cubane-type $S = 5/2$ $[Fe_3S_4]^-$ cluster that results from antiferromagnetic coupling of $S = 2$ Fe^{2+} with $S = 9/2$ $[Fe_2S_2]^+$), cuboidal $S = 2$ $[Fe_3S_4]^0$ ($S = 5/2$ Fe^{3+} antiferromagnetically coupled with $S = 9/2$ $[Fe_2S_2]^+$), $S = 1/2$ $[Fe_4S_4]^+$ ($S = 4$ $[Fe_2S_2]^0$ antiferromagnetically coupled with $S = 9/2$ $[Fe_2S_2]^+$), $S = 3$ or 4 $[Fe_8S_7]^{4+}$ double cubane oxidized nitrogenase P cluster (has the potential to contain a *S*

DOI: 10.1021/jacs.5b01869
J. Am. Chem. Soc. 2015, 137, 4567−4580

= 9/2 $[Fe_2S_2]^+$ fragment in each cubane cluster). In each case a set of low energy bands corresponding to transitions associated with the Fe−Fe interactions of a S = 9/2 valence-delocalized $[Fe_2S_2]^+$ fragment is apparent. The poor resolution of the bands in the $[Fe_8S_7]^{4+}$ P-cluster is tentatively attributed to the overlap of transitions from two slightly different S = 9/2 valence-delocalized $[Fe_2S_2]^+$ fragments. The results demonstrate the potential of VTMCD spectroscopy to identify the presence of valence-delocalized $[Fe_2S_2]^+$ fragments in higher nuclearity Fe−S clusters and to provide a lower limit of the double exchange parameter (B) and thereby the resonance delocalization energies (β) for these fragments via the energies of the primarily $\sigma \rightarrow \sigma^*$ transitions. Consequently the identification and characterization of S = 9/2 valence-delocalized $[Fe_2S_2]^+$ clusters in Cys-to-Ser variants of thioredoxin-like Fds constitutes a major step in understanding both the ground and excited state properties of Fe−S clusters in general.

Finally, we address what the results presented in this work tell us about the origin of valence delocalization in the Cys-to-Ser variants of thioredoxin-like Fd $[Fe_2S_2]^+$ centers and why valence-delocalized $[Fe_2S_2]^+$ clusters are so common in high nuclearity Fe−S clusters but have never been observed thus far in naturally occurring or synthetic $[Fe_2S_2]^+$ clusters. Valence delocalization resulting in an S = 9/2 ground state requires $|B/J| > 9$ in an idealized system in which the two valence-localized configurations have the same energy.[7] This can be accomplished by increasing B, decreasing J, or a combination of both. Asymmetric coordination at the Fe sites and H-bonding interactions involving the bridging sulfides would be expected to decrease J, and this is probably an important contributing factor for observing valence delocalization in the Cys-to-Ser $[Fe_2S_2]$ Fd variants. However, the marked decrease in covalency associated with changing from μ_2-S to μ_3-S bridging sulfides is likely to be the major determinant for lowering J in higher nuclearity Fe−S clusters based on the available S K-edge XAS data.[32,37,39,40] Whether or not B increases substantially in the serinate-coordinated valence-delocalized reduced $[Fe_2S_2]^+$ cluster forms remains to be determined, but clearly B is expected to correlate with the Fe−Fe distance,[29] which has been shown to decrease by 0.04 Å for the oxidized $[Fe_2S_2]^{2+}$ centers in the C55S and C59S variants of *Aae*Fd4 compared to WT.[13] High resolution structural data for reduced WT and the reduced low-pH valence-localized and high-pH valence-delocalized forms of these variants will be required to address the extent to which a decrease in J and/or an increase in B is responsible for valence delocalization. The challenge will be to obtain such data for the high-pH valence-delocalized $[Fe_2S_2]^+$ clusters which only exist as homogeneous species at room temperature, based on the results presented herein.

The ratio of B to the localization energy, ΔE, which contains energetic terms reflecting both the vibronic and static preference for valence localization, is also a major determinant of the degree of valence delocalization. Indeed, a simple resonance Hamiltonian model predicts that valence trapping will generally occur unless $2|B(S + {}^1/_2)| > \Delta E$.[7] We hypothesize that serinate coordination makes the two Fe sites almost isopotential by decreasing the potential at the reducible Fe site by approximately 200 mV at high pH values. This would minimize the static localization energy that corresponds to the energy difference when the extra electron is on Fe_A or Fe_B. Consequently, we propose that the difference in site potentials for the Fe centers in the $[Fe_2S_2]$ clusters and the value of B/J are both a major determinants of the degree of valence (de)localization in $[Fe_2S_2]^+$ centers. Since both of these determinants would be perturbed by changes in H-bonding interactions involving the solvent-exposed serinate and cysteinate ligands, we propose that changes in the H-bonding interactions associated with organization of water molecules at the solvent exposed Fe site in frozen solution are responsible for the valence-delocalized to valence-localized transition on freezing samples for spectroscopic studies.

■ ASSOCIATED CONTENT

Supporting Information

UV−visible absorption spectra of oxidized and dithionite-reduced WT *Aae*Fd4 at pH 7.0 and 11.0 and film voltammograms and oxidative and reductive half-height peak widths as a function of scan rate for C56S *Cp*Fd at high and low pH. This material is available free of charge via the Internet at http://pubs.acs.org.

■ AUTHOR INFORMATION

Corresponding Author

*mkj@uga.edu

Present Addresses

∥S.S.: New Mexico Consortium, 100 Entrada Drive, Los Alamos, NM 87544, U.S.

⊥E.C.D.: Department of Chemistry and Biochemistry, Auburn University, 179 Chemistry Building, Auburn, AL 36849, U.S.

Notes

The authors declare no competing financial interest.

■ ACKNOWLEDGMENTS

This work was supported by grants from the National Institutes of Health (Grant GM62524 to M.K.J.) and the U.K. Engineering Physical Science Research Council (Grant GR/J84809 to F.A.A.)

■ REFERENCES

(1) Achim, C.; Bominaar, E. L.; Munck, E. *J. Biol. Inorg. Chem.* **1998**, *3*, 126.

(2) Bominaar, E. L.; Achim, C.; Borshch, S. A.; Girerd, J.-J.; Münck, E. *Inorg. Chem.* **1997**, *36*, 3689.

(3) Johnson, D. C.; Dean, D. R.; Smith, A. D.; Johnson, M. K. *Annu. Rev. Biochem.* **2005**, *74*, 247.

(4) Beinert, H.; Holm, R. H.; Münck, E. *Science* **1997**, *277*, 653.

(5) Johnson, M. K.; Duin, E. C.; Crouse, B. R.; Golinelli, M.-P.; Meyer, J. In *Spectroscopic Methods in Bioinorganic Chemistry*; Solomon, E. I., Hodgson, K. O., Eds.; American Chemical Society: Washington, DC, 1998; p 286.

(6) Johnson, M. K.; Smith, A. D. In *Encyclopedia of Inorganic Chemistry*, 2nd ed.; King, R. B., Ed.; John Wiley & Sons: Chichester, U.K., 2005; p 2589.

(7) Blondin, G.; Girerd, J.-J. *Chem. Rev.* **1990**, *90*, 1359.

(8) Crouse, B. R.; Meyer, J.; Johnson, M. K. *J. Am. Chem. Soc.* **1995**, *117*, 9612.

(9) Achim, C.; Golinelli, M.-P.; Bominaar, E. L.; Meyer, J.; Münck, E. *J. Am. Chem. Soc.* **1996**, *118*, 8168.

(10) Achim, C.; Bominaar, E. L.; Meyer, J.; Peterson, J.; Münck, E. *J. Am. Chem. Soc.* **1999**, *121*, 3704.

(11) Meyer, J.; Andrade, S. L. A.; Einsle, O. In *Handbook of Metalloproteins 1*; Wiley: Hoboken, NJ, 2008.

(12) Yeh, A. P.; Chatelet, C.; Soltis, S. M.; Kuhn, P.; Meyer, J.; Rees, D. C. *J. Mol. Biol.* **2000**, *300*, 587.

(13) Yeh, A. P.; Ambroggio, X. I.; Andrade, S. L. A.; Einsle, O.; Chatelet, C.; Meyer, J.; Rees, D. C. *J. Biol. Chem.* **2002**, *277*, 34499.

DOI: 10.1021/jacs.5b01869
J. Am. Chem. Soc. 2015, 137, 4567−4580

(14) Fujinaga, J.; Gaillard, J.; Meyer, J. *Biochem. Biophys. Res. Commun.* **1993**, *194*, 104.
(15) Chatelet, C.; Gaillard, J.; Pétillot, Y.; Louwagie, M.; Meyer, J. *Biochem. Biophys. Res. Commun.* **1999**, *261*, 885.
(16) Johnson, M. K. In *Metal Clusters in Proteins*; Que, L., Jr., Ed.; American Chemical Society: Washington, DC, 1988; p 326.
(17) Thomson, A. J.; Cheesman, M. R.; George, S. J. *Methods Enzymol.* **1993**, *226*, 199.
(18) Neese, F.; Solomon, E. I. *Inorg. Chem.* **1999**, *38*, 1847.
(19) Meyer, J.; Fujinaga, J.; Gaillard, J.; Lutz, M. *Biochemistry* **1994**, *33*, 13642.
(20) Werth, M. T.; Cecchini, G.; Manodori, A.; Ackrell, B. A. C.; Schröder, I.; Gunsalus, R. P.; Johnson, M. K. *Proc. Natl. Acad. Sci. U.S.A.* **1990**, *87*, 8965.
(21) Einsle, O.; Andrade, S. L. A.; Dobbek, H.; Meyer, J.; Rees, D. C. *J. Am. Chem. Soc.* **2007**, *129*, 2210.
(22) Bertrand, P.; Gayda, J.-P. *Biochim. Biophys. Acta* **1979**, *579*, 107.
(23) Bertrand, P.; Guigliarelli, B.; Gayda, J.-P.; Beardwood, P.; Gibson, J. F. *Biochim. Biophys. Acta* **1985**, *831*, 261.
(24) Orio, M.; Mouesca, J. M. *Inorg. Chem.* **2008**, *47*, 5394.
(25) Fu, W.; Drozdzewski, P. M.; Davies, M. D.; Sligar, S. G.; Johnson, M. K. *J. Biol. Chem.* **1992**, *267*, 15502.
(26) Thomson, A. J.; Cammack, R.; Hall, D. O.; Rao, K. K.; Briat, B.; Rivoal, J. C.; Badoz, J. *Biochim. Biophys. Acta* **1977**, *493*, 132.
(27) Norman, J. G.; Kalbacher, B. J.; Jackels, S. C. *J. Chem. Soc., Chem. Commun.* **1978**, 1027.
(28) Summerville, R. H.; Hoffmann, R. *J. Am. Chem. Soc.* **1976**, *98*, 7240.
(29) Gamelin, D. R.; Bominaar, E. L.; Kirk, M. L.; Wieghardt, K.; Solomon, E. I. *J. Am. Chem. Soc.* **1996**, *118*, 8085.
(30) Morales, R.; Chron, M.-H.; Hudry-Clergeon, G.; Pétillot, Y.; Norager, S.; Medina, M.; Frey, M. *Biochemistry* **1999**, *38*, 15764.
(31) Noodleman, L.; Case, D. A. *Adv. Inorg. Chem.* **1992**, *38*, 423.
(32) Dey, A.; Glaser, T.; Moura, J. J. G.; Holm, R. H.; Hedman, B.; Hodgson, K. O.; Solomon, E. I. *J. Am. Chem. Soc.* **2004**, *126*, 16868.
(33) Kröckel, M.; Grodzicki, M.; Papaefthymiou, V.; Trautwein, A. X.; Kostikas, A. *J. Biol. Inorg. Chem.* **1996**, *1*, 173.
(34) Blondin, G.; Girerd, J.-J. *J. Biol. Inorg. Chem.* **1996**, *1*, 170.
(35) Noodleman, L.; Case, D. A.; Mouesca, J.-M. *J. Biol. Inorg. Chem.* **1996**, *1*, 177.
(36) Bertini, I.; Luchinat, C. *J. Biol. Inorg. Chem.* **1996**, *1*, 183.
(37) Solomon, E. I.; Xie, X.; Dey, A. *Chem. Soc. Rev.* **2008**, *37*, 623.
(38) Gamelin, D. R.; Bominaar, E. L.; Mathonière, C.; Kirk, M. L.; Wieghardt, K.; Girerd, J.-J.; Solomon, E. I. *Inorg. Chem.* **1996**, *35*, 4323.
(39) Anxolabéhère-Mallart, E.; Glaser, T.; Frank, P.; Aliverti, A.; Zanetti, G.; Hedman, B.; Hodgson, K. O.; Solomon, E. I. *J. Am. Chem. Soc.* **2001**, *123*, 5444.
(40) Dey, A.; Glaser, T.; Couture, M. M. J.; Eltis, L. D.; Holm, R. H.; Hedman, B.; Hodgson, K. O.; Solomon, E. I. *J. Am. Chem. Soc.* **2004**, *126*, 8320.

DOI: 10.1021/jacs.5b01869
J. Am. Chem. Soc. 2015, 137, 4567−4580